© 2018. Published by The Company of Biologists Ltd | Development (2018) 145, dev158931. doi:10.1242/dev.158931

RESEARCH ARTICLE

Polycystin 1 loss of function is directly linked to an imbalance in G-protein signaling in the kidney

Bo Zhang[1,2,*], Uyen Tran[1] and Oliver Wessely[1,‡]

ABSTRACT

The development of the kidney relies on the establishment and maintenance of a precise tubular diameter of its functional units, the nephrons. This process is disrupted in polycystic kidney disease (PKD), resulting in dilations of the nephron and renal cyst formation. In the course of exploring G-protein-coupled signaling in the *Xenopus* pronephric kidney, we discovered that loss of the G-protein α subunit, Gnas, results in a PKD phenotype. Polycystin 1, one of the genes mutated in human PKD, encodes a protein resembling a G-protein-coupled receptor. Furthermore, deletion of the G-protein-binding domain present in the intracellular C terminus of polycystin 1 impacts functionality. A comprehensive analysis of all the G-protein α subunits expressed in the *Xenopus* pronephric kidney demonstrates that polycystin 1 recruits a select subset of G-protein α subunits and that their knockdown – as in the case of Gnas – results in a PKD phenotype. Mechanistically, the phenotype is caused by increased endogenous G-protein β/γ signaling and can be reversed by pharmacological inhibitors as well as knocking down Gnb1. Together, our data support the hypothesis that G proteins are recruited to the intracellular domain of PKD1 and that this interaction is crucial for its function in the kidney.

KEY WORDS: Polycystic kidney disease, Pronephros, *Xenopus*, Adhesion GPCR

INTRODUCTION

The kidney is responsible for the excretion of waste products, but also for controlling water and solute homeostasis (Smith, 1953; Saxén, 1987; Vize et al., 2003). The performance and longevity of the kidney is contingent on the number and correct development of its functional units, the nephrons (Bertram et al., 2013). Nephrons form in a highly stereotypical fashion, generating several functionally distinct cell types along its proximal-distal axis (Desgrange and Cereghini, 2015; McMahon, 2016). In addition, nephrons are characterized by a precisely defined tubule diameter that maximizes channel, transporter and receptor-mediated water and solute reabsorption (Fischer et al., 2006; Karner et al., 2009; Lienkamp et al., 2012; Wessely et al., 2014).

The control of tubule diameter is disrupted in polycystic kidney diseases. This group of genetically inherited human disorders is characterized by the formation of fluid-filled kidney cysts as a result of a disrupted nephron diameter control, ultimately leading to end-stage renal disease (Harris and Torres, 2009; Grantham et al., 2011; Chebib and Torres, 2016). The genes mutated in its most common form, autosomal dominant polycystic kidney disease (ADPKD), are *PKD1* and *PKD2* (Hughes et al., 1995; The International Polycystic Kidney Disease Consortium, 1995; Mochizuki et al., 1996). Polycystin 1 (PKD1) encodes a large transmembrane protein and polycystin 2 (PKD2) is a member of the transient receptor potential (TRP) superfamily. The two proteins are believed to interact and regulate intracellular Ca^{2+} levels. However, the molecular mechanisms underlying the cellular changes that lead to cyst formation and expansion in response to loss of PKD1 are not well understood. Recent studies have focused on the intracellular C-terminal tail of polycystin 1, which binds multiple signaling proteins and is subjected to proteolytic cleavage, generating a fragment that can enter the nucleus (Chauvet et al., 2004; Low et al., 2006; Merrick et al., 2012). Another intriguing aspect of PKD1 is that it has hallmarks of a G-protein-coupled receptor (GPCR). Although it lacks the typical seven transmembrane domain configuration, the intracellular C-terminus harbors a G-protein binding domain (GBD), which binds to multiple G α subunits (Parnell et al., 1998, 2002; Delmas et al., 2002; Yu et al., 2010, 2011). Moreover, the extracellular N terminus contains an evolutionarily conserved GPCR auto-proteolysis site (GPS) involved in PKD1 sorting and function (Cai et al., 2014; Kurbegovic et al., 2014; Qian, 2015; Su et al., 2015; Trudel et al., 2016). In fact, the GPS motif is part of a larger domain, the GPCR autoproteolysis-inducing (GAIN) domain (Prömel et al., 2013; Trudel et al., 2016). This domain is one of the defining features of the adhesion GPCRs, a subgroup of at least 33 GPCRs in humans, the overarching function of which is still poorly described although they may act as autonomous adhesive and signaling units (Prömel et al., 2013). Despite these efforts, it is still unclear whether PKD1 indeed functions as a GPCR.

The molecular mechanisms underlying PKD are studied in many model organisms (Torres and Harris, 2007; Happé and Peters, 2014). The African clawed frog, *Xenopus laevis*, has emerged as a powerful alternative system due to the formation of functional kidneys 48 h post fertilization and the ease with which high-throughput knockdown studies can be performed (Wessely and Obara, 2008; White et al., 2010; Wessely and Tran, 2011). Here, we have used these advantages to investigate the function of polycystin 1 (Pkd1). We now demonstrate that the crucial feature of polycystin 1 with respect to its loss-of-function phenotype is its ability to bind trimeric G proteins. In a systematic approach examining the entire family of G-protein α subunits, we show that Pkd1 binds a subset of G-protein α subunits and restricts their signaling ability. In the absence of Pkd1, G-protein α- and β/γ-dependent signals become

[1]Cleveland Clinic Foundation, Lerner Research Institute, Department of Cellular and Molecular Medicine, 9500 Euclid Avenue/NC10, Cleveland, OH 44195, USA. [2]LSU Health Sciences Center, Department of Cell Biology and Anatomy, 1901 Perdido Street, New Orleans, LA 70112, USA.
*Present Address: Tianjin Medical University, School of Basic Medical Sciences, Department of Immunology, Tianjin Key Laboratory of Cellular and Molecular Immunology, Tianjin, People's Republic of China.

‡Author for correspondence (wesselo@ccf.org)

B.Z., 0000-0002-1359-9820; O.W., 0000-0001-6440-7975

Received 31 August 2017; Accepted 1 March 2018

Development (2018) 145, dev158931. doi:10.1242/dev.158931

hyper-activated, contributing to the complex cellular phenotype seen in cystic renal epithelial cells. These data provide a novel angle towards treating ADPKD.

RESULTS

Gnas knockdown results in a PKD phenotype

The *Xenopus* PKD phenotype is characterized by the formation of edema due to impaired kidney function, dilated pronephric tubules and ducts, and the loss of the expression of the sodium bicarbonate co-transporter *Nbc1* in the late distal tubule (Tran et al., 2007, 2010). In the course of examining the effect of cholera toxin on trimeric G-protein signaling during proximal tubular growth (Zhang et al., 2013), we discovered that knockdown of *Gnas*, but not *Gnal*, resulted in a PKD phenotype very reminiscent of the one observed when the PKD genes polycystin 1 or polycystin 2 were knocked down (Tran et al., 2007, 2010; Xu et al., 2015; Kim et al., 2016). Microinjection of an antisense morpholino oligomer targeting *Gnas* (*Gnas-MO*) caused edema, the dilation of the pronephric tubules and ducts and the loss of the expression of the sodium bicarbonate co-transporter *Nbc1* in the late distal tubule (Figs 1A-F, 2A-C and Fig. S1). Interestingly, one of the many hypotheses for the mechanism of action of polycystin 1 (PKD1) is that it acts as an atypical G-protein-coupled receptor (GPCR) (Parnell et al., 1998; Yuasa et al., 2004; Hama and Park, 2016). A sequence comparison between *Xenopus* and human PKD1 revealed that the previously described G-protein-binding domain (GBD) is more than 90% conserved at the amino acid level between human and frog (Fig. 1G and Fig. S2A). Thus, we decided to address whether the *Gnas* morphant phenotype could be explained by a direct link between trimeric G-proteins and PKD1. To assess this, we used a paradigm previously reported in zebrafish (Merrick et al., 2012), i.e. the rescue of the Pkd1 morphant phenotype by the Pkd1 C-terminal tail. As we have shown (Xu et al., 2015; Kim et al., 2016), eliminating Pkd1 in *Xenopus* embryos using an antisense morpholino oligomer (*Pkd1-sMO*) results in a PKD phenotype (Fig. 1H,I,L and data not shown). As expected, co-injection of synthetic mRNA encoding the intracellular C-terminal tail of *Xenopus* Pkd1 (*Pkd1-CTT*) was sufficient to rescue the late distal tubular expression of *Nbc1* (Fig. 1J,L). To address, whether the GBD is involved, we next deleted the five core amino acids of the Pkd1 GBD, RKKVR (Fig. S2A), and co-injected this construct (*Pkd1-CTTΔGBD*) with the *Pkd1-sMO*. As shown in Fig. 1K,L, this mRNA could not restore the staining of *Nbc1* in the late distal tubule. The sequence of the Pkd1 GBD overlaps with nuclear localization sequence (NLS) described by Chauvet et al. (2004) (Fig. S2A). Thus, we wondered whether *Pkd1-CTTΔGBD* exhibits changes in the subcellular localization. HEK293T cells were transiently transfected with a Myc-tagged version of *Pkd1-CTT* and *Pkd1-CTTΔGBD*, and processed for immunofluorescence analyses. As shown in Fig. S2B,C, both proteins localized to the nucleus. This implies that the G-protein-binding activity and not the nuclear localization of Pkd1-CTT is crucial for its rescue of the Pkd1 morphants. Together, these data suggest that an interaction between Gnas and Pkd1 may be a crucial aspect of Pkd1 function in the kidney.

Comprehensive analysis of G-protein α subunits

Previous studies have demonstrated that PKD1 can bind multiple G-protein α subunits (Parnell et al., 1998, 2002; Delmas et al., 2002; Yu et al., 2010, 2011). To better understand how Pkd1 could modulate trimeric G-protein signaling in the *Xenopus* kidney, we decided to identify which G-protein α subunits are expressed in the pronephric kidney. To achieve this, we systematically analyze the expression of all G-protein α subunits. RNAseq data indicated that the entire G-protein α family is expressed in stage 39 *Xenopus* embryos (Fig. S3A). The only exception was *Gna12*, which we could not identify in the *Xenopus* genome. Next, we performed whole-mount *in situ* hybridization covering all phases of *Xenopus* kidney development (Fig. S3B-O′ and data not shown). As expected, the G-protein α family exhibited very diverse expression patterns, with some members appearing rather ubiquitous, while others were much more restricted (e.g. Gnat2 staining in the eye and the pineal gland).

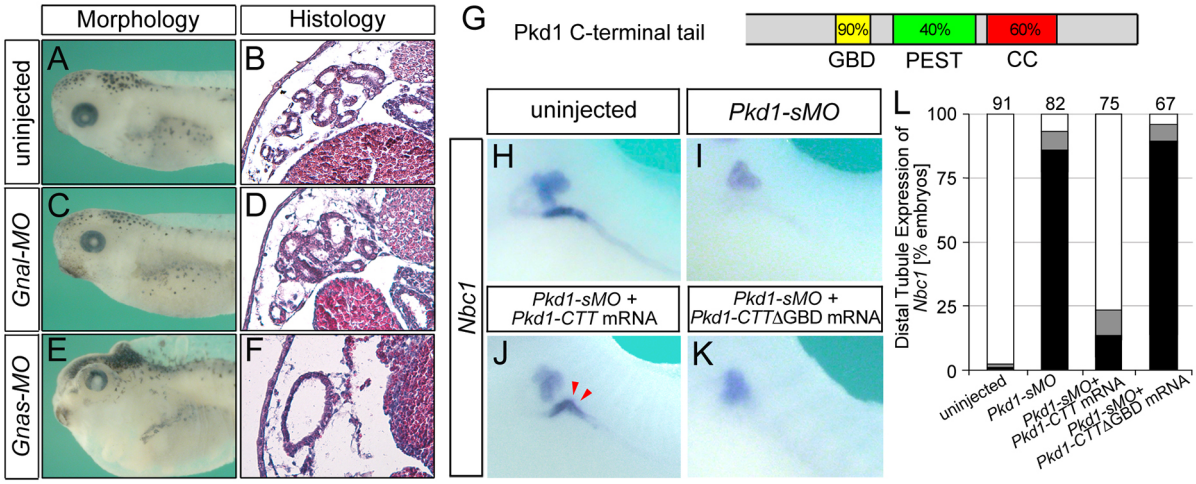

Fig. 1. Interfering with G-protein binding of Pkd1 results in a PKD phenotype. (A-F) *Xenopus* embryos injected with *Gnal-MO* or *Gnas-MO* and uninjected control embryos were analyzed morphologically and histologically at stage 42. (G) Schematic of the Pkd1 C-terminal tail (CTT) indicating the three conserved domains: the G-protein binding (GBD), the PEST and the coiled-coil domain (CC). The percentage identity between the *Xenopus* and human protein for each domain is indicated. (H-L) Uninjected controls and embryos injected with *Pkd1-sMO* alone or co-injected with *Pkd1-CTT* or *Pkd1-CTTΔGBD* mRNA were analyzed by *Nbc1* whole-mount *in situ* hybridization at stage 39. The rescue of *Nbc1* in the late distal tubule upon injection of the *Pkd1-CTT* mRNA is indicated by red arrowheads. (L) Quantification of three independent experiments with white bars indicating normal expression, gray bars reduced expression and black bars absent expression. The number of embryos examined is indicated above each bar. The data are presented as cumulative numbers of at least three biological replicas.

Development (2018) 145, dev158931. doi:10.1242/dev.158931

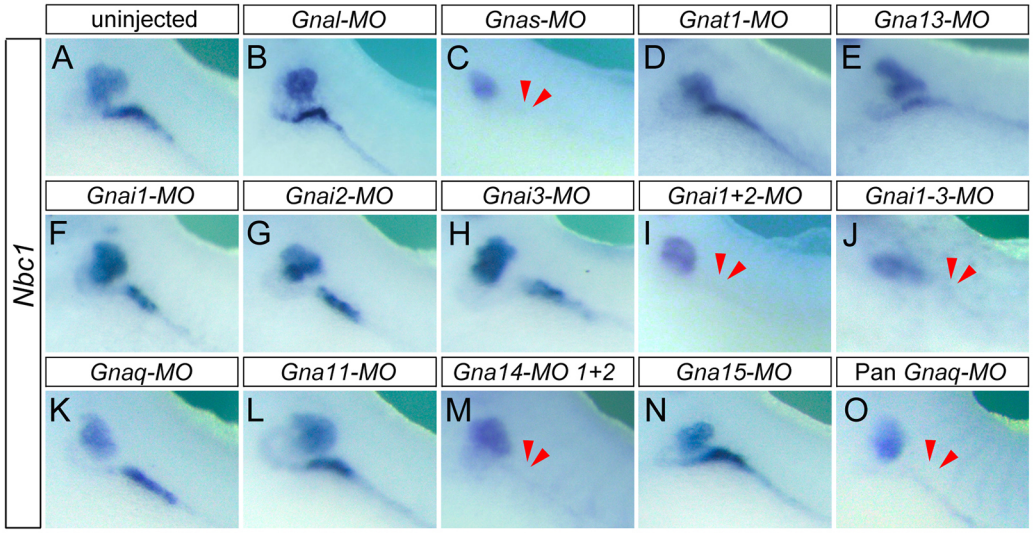

Fig. 2. Systematic analysis of the knockdown phenotypes of G-protein α subunits and their interaction with polycystin 1. (A-O) Whole-mount *in situ* hybridization for *Nbc1* expression comparing embryos lacking individual G-protein α subunits or combinations thereof. Representative images are shown. Loss of *Nbc1* expression in the late distal tubule is indicated by red arrowheads.

However, with respect to the kidney, only *Gnao* and *Gnat2* could not be detected in the developing pronephros.

We next focused on these G-protein α subunits and designed antisense morpholino oligomers (MOs) against each of them that targeted, if possible, both homeologs with a single MO (with the exception of Gna14, which required two, see Table S1). MOs were validated by *in vitro* transcription/translation (Fig. S4). As in the case of Gnas, the MOs were injected individually into *Xenopus* embryos and analyzed for the occurrence of a PKD phenotype. Moreover, we tested for potential functional redundancy. G-protein α subunits are classified into four families based on their mode of downstream signaling (Neves et al., 2002; Dorsam and Gutkind, 2007). To account for compensation within these families, we performed combinatorial knockdowns that eliminated two or three family members simultaneously. Surprisingly, among all the combinations tested, only a small subset fulfilled all three criteria for the PKD phenotype, i.e. the occurrence of edema, dilations of the kidney tubules and loss-of-expression of *Nbc1* in the late distal tubule (Fig. 2). These were the knockdown of Gnas, the knockdown of Gna14 (a Gnaq family member) and the combined knockdown of the two Gnai family members, Gnai1 and Gnai2 (Table 1).

Based on this unexpected specificity, we wondered whether a correlation exists between the PKD knockdown phenotype of G-protein α subunits and their ability to bind to Pkd1. Several G-protein α subunits have been shown to bind to PKD1 (Parnell et al., 1998, 2002; Delmas et al., 2002; Yu et al., 2010, 2011). Yet these studies have never addressed all G-protein α subunits, nor have they determined binding affinities. To achieve this, we performed surface plasmon resonance (SPR) analysis using bacterially purified Pkd1-CTT and reticulocyte lysate-produced G-protein α subunits. Only four *Xenopus* α subunits (Gnas, Gna14, Gnai1 and Gnai2), as well as mouse Gna12 [which has been shown to interact with Pkd1 (Yuasa et al., 2004), but has yet to be identified in the *Xenopus* genome] exhibited high binding affinities (Fig. 3A,A′). This interaction was independent of which partner was immobilized on the chip (Fig. S5). However, it was dependent on the G-protein-binding domain, because high-affinity binding was abolished when the Pkd1-CTTΔGBD protein was used instead (Fig. 3B,B′). Importantly, the calculated binding affinities (Fig. 3A′,B′) were in a similar range to the binding of the G-protein α subunits to GPCRs (Komolov et al., 2006). In summary, these analyses demonstrate a striking correlation between G-protein α subunits that exhibit high-affinity binding to Pkd1 and those exhibiting the PKD phenotype upon knockdown in *Xenopus*.

Analysis of G-protein signaling

The results so far are in agreement with the hypothesis that Pkd1 functions as a GPCR that signals via a distinct set of G proteins and activates α- and/or β/γ-dependent signaling cascades (Fig. 4A). To test this, we aimed to restore G-protein signaling in Pkd1 morphants. Morphant embryos and untreated controls were incubated with

Table 1. The phenotypes of *Xenopus* embryos lacking G-protein α subunits either individually or in combination

			Nbc1 expression in late distal tubule		
	Edema	Dilated tubules	Normal	Reduced	Absent
Uninjected control	0%	No	99%	0%	0%
*Gnas-MO**	99%	Yes	5%	10%	85%
Gnal-MO	82%	No	94%	6%	0%
Gnai1-MO	23%	No	70%	15%	15%
Gnai2-MO	26%	No	73%	12%	15%
Gnai3-MO	5%	No	90%	10%	0%
*Gnai1+2-MO**	95%	Yes	3%	11%	86%
Gnai1+3-MO	26%	No	70%	14%	16%
Gnai2+3-MO	29%	No	73%	13%	14%
*Gnai1+2+3-MO**	98%	Yes	6%	4%	90%
Gnat1-MO	10%	No	90%	8%	1%
Gna13-MO	11%	No	85%	11%	4%
Gnaq-MO	8%	No	91%	4%	5%
Gna11-MO	8%	No	93%	3%	4%
*Gna14-MO 1+2**	91%	Yes	6%	12%	82%
Gna15-MO	14%	No	83%	6%	11%
Gnaq+11+15-MO	55%	Yes	55%	11%	34%
Pan *Gnaq*-MO*	98%	Yes	9%	4%	87%

*Morphants with a PKD phenotype.

Pan *Gnaq-MO* stands for the knockdown of the entire Gnaq family by simultaneous injection of *Gnaq-MO*, *Gna11-MO*, *Gna14-MO1+2* and *Gna15-MO*. The data are presented as percentages of at least three biological replicas.

Development (2018) 145, dev158931. doi:10.1242/dev.158931

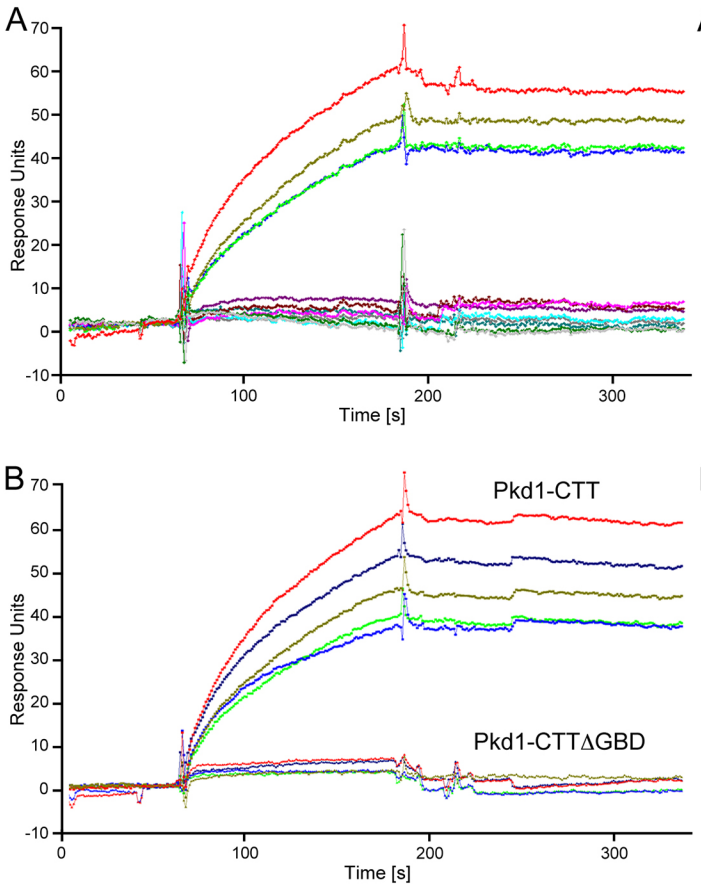

A'

	Subunit	K_D(M)
Pkd1-CTT	Gnas	$1.46x10^{-10}$
	Gna14	$1.00x10^{-9}$
	Gnai1	$2.39x10^{-9}$
	Gnai2	$2.56x10^{-9}$
	Gnai3	$1.76x10^{-8}$
	Gna15	$1.69x10^{-8}$
	Gnaq	$1.45x10^{-7}$
	Gnat1	$1.69x10^{-7}$
	Gna11	$1.77x10^{-7}$
	Gnaz	$3.84x10^{-7}$
	Gnal	$4.48x10^{-7}$
	Gna13	$7.14x10^{-7}$

B'

	Subunit	K_D(M)
Pkd1-CTT	Gnas	$1.47x10^{-10}$
	mGna12	$5.35x10^{-10}$
	Gnai14	$1.07x10^{-9}$
	Gnai1	$2.31x10^{-9}$
	Gnai2	$2.98x10^{-9}$
Pkd1-CTTΔGBD	Gnas	$3.00x10^{-4}$
	mGna12	$3.50x10^{-4}$
	Gnai14	$3.90x10^{-4}$
	Gnai1	$6.80x10^{-4}$
	Gnai2	$7.20x10^{-4}$

Fig. 3. Surface plasmon resonance analysis of the interaction between G-protein α subunits with the polycystin 1 C-terminal tail. (A,A′) SPR analysis between the C-terminal tail of Pkd1 (Pkd1-CTT) and the different G-protein α subunits expressed in the pronephros of *Xenopus* embryos. (A) A representative sensorgram and (A′) a table of the equilibrium dissociation constants [K_D (M)] for each interaction. (B,B′) SPR analysis between G-protein α subunits and Pkd1-CTT or Pkd1-CTTΔGBD proteins. (B) A representative sensorgram and (B′) a table of the equilibrium dissociation constants [K_D (M)] for each interaction. This analysis not only includes the *Xenopus* G-protein α subunits with high binding affinity, but also mouse Gna12, which has been shown to interact with Pkd1 (Parnell et al., 1998; Yuasa et al., 2004).

low molecular weight compounds that activate or inhibit effector molecules downstream of trimeric G proteins. As Gnas activates cyclic AMP (cAMP), we raised cAMP levels using the adenylate cyclase activator forskolin or two cAMP analogs: the PKA-specific 6-Bnz-cAMP-AM (cAMP-PKA) and the Rapgef3/4-specific 8-pCPT-2′-O-Me-cAMP-AM (cAMP-Epac). However, none of the compounds could rescue the PKD phenotype (Fig. 4C and data not shown). Similarly, mimicking Gnai family activity by inhibiting cAMP signaling using the protein kinase A (PKA) inhibitor H89, the Rapgef3/4 inhibitor brefeldin A (BFA) or by injecting the *Rapgef4-MO* (Zhang et al., 2013) did not have any effect (Fig. 4D). Next, we mimicked Gna14 signaling by stimulating its effector phospholipase C β (PLCβ) using m-3M3FBS, but did not observe a reversal of the Pkd1 morphant phenotype either (Fig. 4E).

G-proteins signal not only via α subunit-dependent pathways but also via β/γ subunits (Smrcka, 2008; Hama and Park, 2016). To test whether inhibiting β/γ signaling, like the loss of G-protein α signaling, induced a PKD phenotype in *Xenopus* embryos, we used two compounds (Fig. 4A). We either exposed embryos to the G-protein β/γ 'hot-spot' inhibitor gallein (Lin and Smrcka, 2011) or blocked PLCβ, a direct target of G-protein β/γ signaling, with U73122. However, neither method impacted *Nbc1* staining in the late distal tubule of the kidney (Fig. 4F,G,J).

As re-activation of downstream G-protein signaling was insufficient to restore the Pkd1 morphant phenotype, we envisioned an alternative explanation: a model based on competition for G-protein β/γ subunits (Fig. 4B). It is based on the fact that trimeric G-proteins function as mixed pools of α and β/γ subunits, where the β/γ subunits are shared between the different α subunits (Smrcka, 2008). We hypothesize that the absence of Pkd1 increases the pool of free G-protein β/γ subunits. They are then available to signal either in complex with other α subunits or even by themselves. To test this hypothesis, we inhibited β/γ-dependent signaling in Pkd1 morphants and observed a very dramatic effect (Fig. 4F-J). Both gallein and U73122 restored *Nbc1* expression in *Pkd1-sMO*-injected embryos. As gallein efficacy is quite batch dependent (see Materials and Methods) and PLCβ signaling is also regulated by Gna14 (Fig. 4A), we decided to verify the observation by directly eliminating G-protein β/γ signaling. As in the case of the G-protein α subunits, we surveyed the five known G-protein β subunits for expression in the developing pronephros (Fig. S6A,C-G′ and data not shown). Among those, *Gnb1* displayed the most prominent pronephric kidney expression. An antisense morpholino oligomer targeting Gnb1 (*Gnb1-MO*) efficiently blocked *Gnb1* mRNA translation. It did not result in any overt phenotypes when injected on its own (Figs 4J, 5E and Fig. S6B). However, when co-injected with the *Pkd1-sMO*, the double morphants exhibited restored *Nbc1* expression and did not develop edema (Figs 4J and 5E), thus supporting our competition model.

To further strengthen this, we tested another paradigm associated with renal cyst formation: the randomization of the angle of cell division in renal tubules (Fischer et al., 2006; Nishio et al., 2010; Fedeles and Gallagher, 2013). Unfortunately, direct imaging of mitotic figures in the *Xenopus* pronephric kidney was impractical owing to the low number of cell divisions (Romaker et al., 2014; data not shown). Thus, we opted for a pulse-labeling approach that followed the fate of cells post cell division, analyzing whether dividing cells are found along the length of the tubule or circumferential to it. To achieve this, embryos were injected with 5-ethynyl-2′-deoxyuridine (EdU) at stage 40, fixed at stage 42 and

Development (2018) 145, dev158931. doi:10.1242/dev.158931

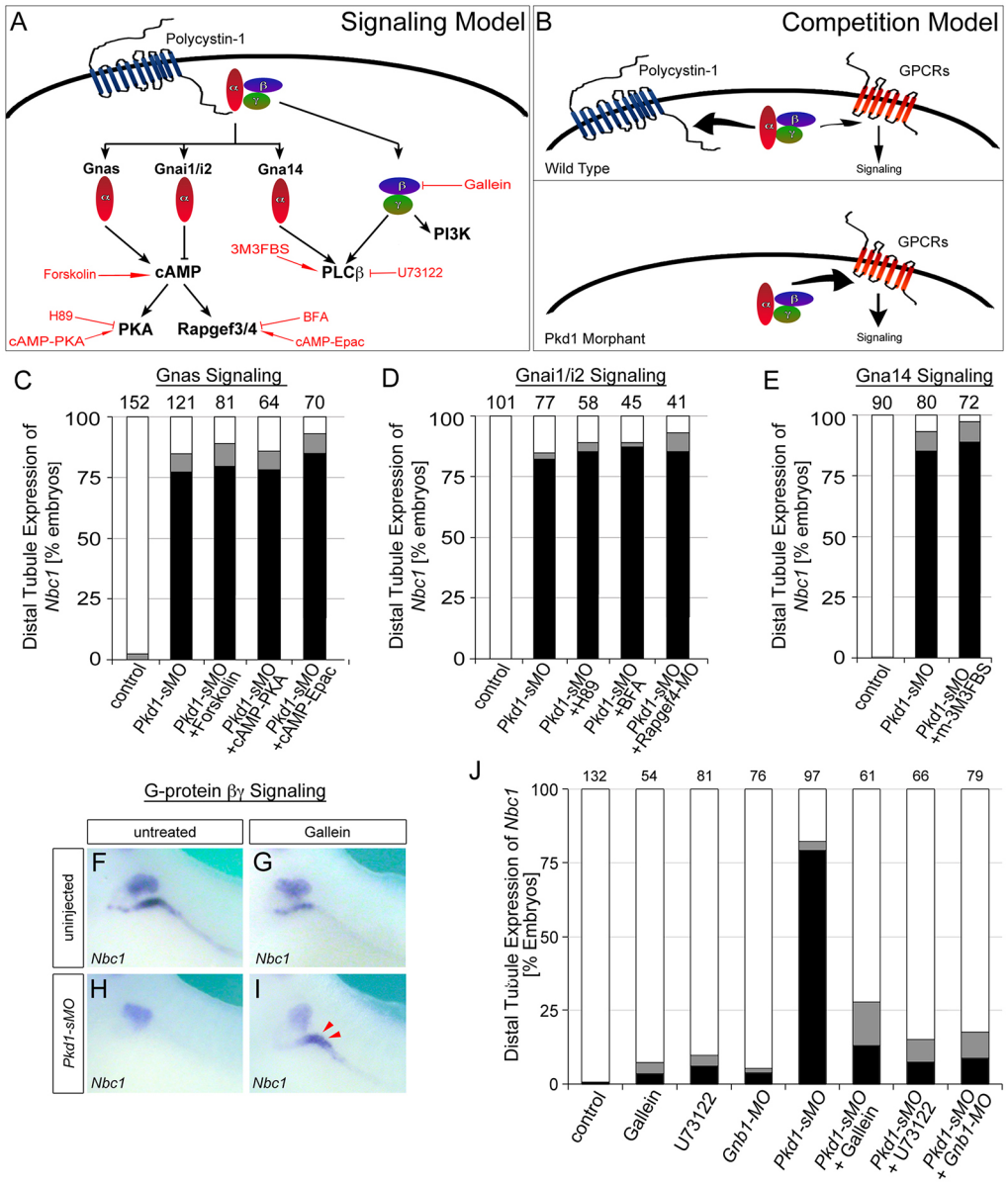

Fig. 4. Connection between polycystin 1 and G-protein signaling in *Xenopus*. (A) Signaling model depicting Pkd1 acting as a GPCR. The four G-protein α subunits that bind Pkd1, the shared G-protein β/γ complex and key downstream signaling components for each are depicted. Compounds used to activate or inhibit the different signaling pathways are highlighted in red. (B) Competition model describing how the presence of Pkd1 (upper panel) or its absence (lower panel) would affect signaling via other GPCRs. (C-E) Bar graphs showing that activating Gnas-dependent (C), Gnai1/2-dependent (D) and Gna14-dependent (E) signaling in Pkd1 morphants does not rescue the distal tubular expression of *Nbc1*; *Pkd1-sMO*-injected embryos were treated with 20 µM forskolin, 150 ng/ml of the PKA-specific cAMP analogue 6-Bnz-cAMP-AM (cAMP-PKA), 100 ng/ml of the Rapgef3/4-specific cAMP analogue 8-pCPT-2′-O-Me-cAMP-AM (cAMP-Epac), 20 µM H89, 200 ng/ml brefeldin A (BFA) and 100 µM m-3M3FBS. To test the contribution of Rapgef4, the two MOs were co-injected. (F-I) Uninjected controls and embryos injected with *Pkd1-sMO* in the presence or absence of 20 µM gallein were analyzed by *Nbc1* whole-mount *in situ* hybridization at stage 39. The restoration of *Nbc1* staining in the late distal tubule upon treatment with gallein is indicated by red arrowheads. (J) Bar graph summarizing the effect of gallein (20 µM), U73122 (1 µg/ml) treatment or co-injection of *Gnb1-MO* on *Nbc1* expression in wild-type controls or Pkd1 morphants. Each of the bar graphs summarizes the quantification of at least three independent experiments, with white bars indicating normal expression, gray bars reduced expression and black bars absent expression of *Nbc1* in the late distal tubule. The number of embryos examined is indicated above each bar. The data are presented as cumulative numbers of at least three biological replicas.

analyzed for the presence of labeled cell doublets in transverse or sagittal sections (Fig. 5F,G). In line with data in mouse and zebrafish (Fischer et al., 2006; Bubenshchikova et al., 2012), control embryos displayed a preference of dividing cells ending up aligned along the length of the nephron (Fig. 5H). Conversely, *Pkd1* or *Gnas* morphants displayed the opposite distribution with cells integrating rather circumferentially. Treating *Pkd1-sMO* or *Gnas-MO*-injected embryos with gallein or co-injecting the *Gnb1-MO* reversed the phenotype and the cell division profile was similar to the one observed for control embryos.

Based on these data, we propose that the absence of Pkd1 in *Xenopus* results in unbalanced G-protein signaling, which is causally involved in the formation of the amphibian PKD phenotype. In humans, ADPKD is caused by mutations in either PKD1 or PKD2, and it is generally thought that the two proteins form an interdependent complex (Torres et al., 2007). Thus, we wondered

Development (2018) 145, dev158931. doi:10.1242/dev.158931

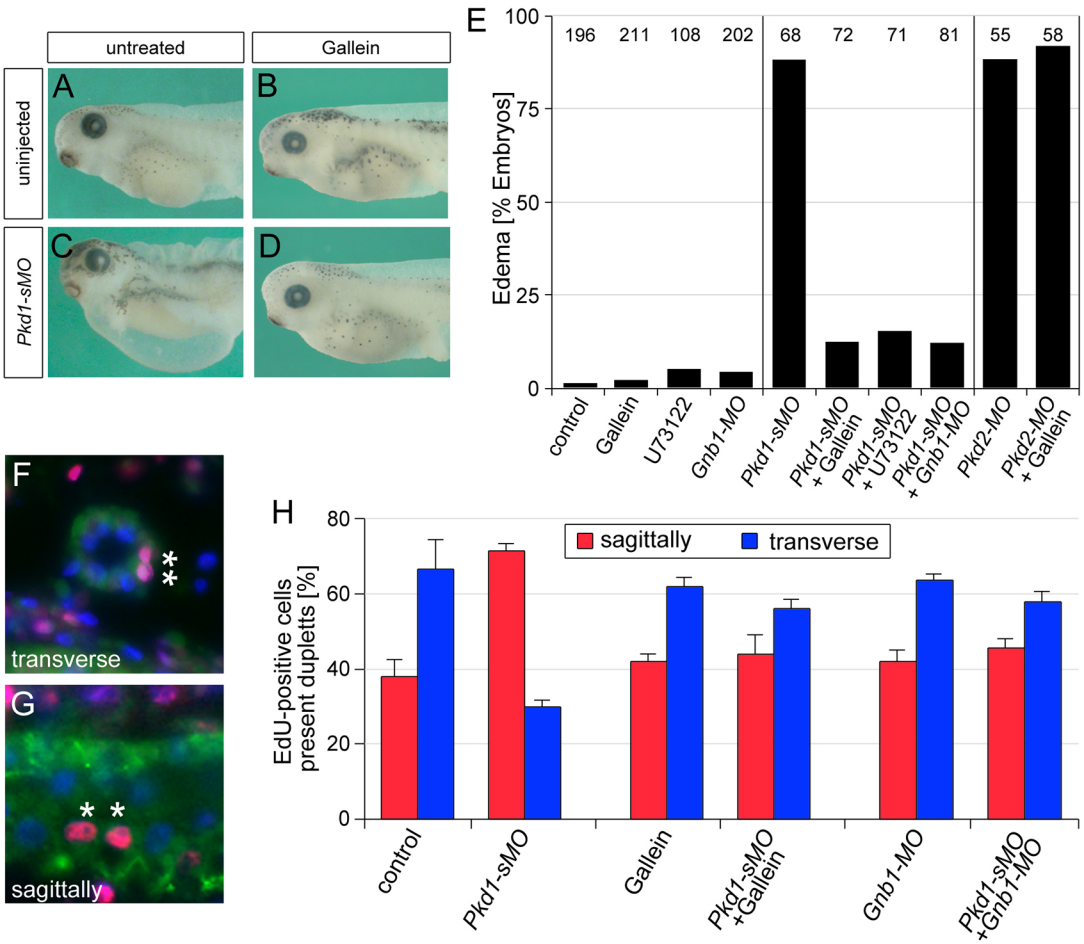

Fig. 5. Loss of polycystin 1 and G-protein β/γ signaling in *Xenopus*. (A-D) Uninjected controls and embryos injected with *Pkd1-sMO* in the presence or absence of 20 µM gallein were analyzed by morphology at stage 42. (E) Bar graph summarizing the effect of gallein (20 µM) and U73122 (1 µg/ml) treatment or co-injection of *Gnb1-MO* on edema formation in wild-type controls, Pkd1 and Pkd2 morphants. The bar graph summarizes the results of more than three independent experiments; the numbers of embryos analyzed are depicted at the top of each bar. (F-H) The plane of cell division was assayed by pulse labeling of dividing cells using EdU at stage 40. Transverse and sagittal sections were analyzed at stage 42 for the appearance of a pair of EdU-labeled daughter cells (red). (F,G) Representative images with the two EdU-positive daughter cells indicated by asterisks. The pronephric kidney was visualized by Na/K-ATPase staining (green) and nuclei were counterstained with DAPI (blue). Data from at least three biologically independent experiments are summarized in H. Error bars indicate s.d. Kidney cells from uninjected controls divide more sagittally than transversely. Embryos exhibiting a PKD phenotype increase the number of transverse cell divisions, whereas gallein or the co-injection of a *Gnb1-MO* restores the original distribution. The percentages do not add up to 100, as cell duplets had to be present in the respective sections.

whether hyperactivation of G-proteins is a general consequence of a PKD phenotype and also underlies the Pkd2 loss-of-function phenotype. However, when we analyzed *Xenopus* embryos injected with a *Pkd2-MO* treated with or without gallein, edema formation was not rescued upon gallein exposure (Fig. 5E). Therefore, the competition model is only observed for Pkd1, but not Pkd2, suggesting that Pkd2 functions downstream or parallel of Pkd1.

Loss of Pkd1 results in hyperactivation of G-protein signaling

All experiments so far were performed using *Xenopus*. To test the wider applicability of our model, we decided to use a mammalian cell culture system, two isogenic proximal tubular cell lines generated from *Pkd1* floxed mice ($Pkd1^{Fl/-}$ and $Pkd1^{-/-}$) (Shibazaki et al., 2008). As previously reported (Merrick et al., 2012), these cells mimic the cystogenic potential seen *in vivo*. When grown under 3D culture conditions in matrigel at the non-permissive temperature of 37°C, the $Pkd1^{Fl/-}$ cells form tubular structures and the $Pkd1^{-/-}$ cells form cysts (Fig. 6A,E). In agreement with the *Xenopus* data, treating the Pkd1 mutant cells with the β/γ inhibitor gallein interfered with the cyst formation and resulted in a conversion to more tubular structures (Fig. 6B,F).

Upregulation of cyclic AMP (cAMP) is a central aspect of the pathogenesis of PKD and is believed to contribute both to increased fluid secretion and proliferation in cystic epithelia (Calvet, 2015). Although it is generally thought to be an indirect mechanism, our competition model (Fig. 4B) suggests that not only β/γ, but also α signaling should be activated by the absence of Pkd1. To achieve this, we exposed cells to the PKA inhibitor H89 (Fig. 6C,G). Although H89 had no discernible effect on the control cells, it reduced cyst size of the Pkd1-null cells. Moreover, the combination of both H89 and gallein was at least additive (Fig. 6D,H). Interestingly, an upregulation of PKA signaling would have been missed in *Xenopus*, as the inhibition of PKA does not impact kidney development (Zhang et al., 2013).

We also measured another parameter of cystogenesis: cell growth. When switched to the non-permissive temperature of 37°C, control cells barely proliferated. Conversely, Pkd1 mutant cells continued to divide (Fig. 6I,J). Addition of gallein or H89 reduced cell proliferation, with gallein being more potent than H89. However, the

Development (2018) 145, dev158931. doi:10.1242/dev.158931

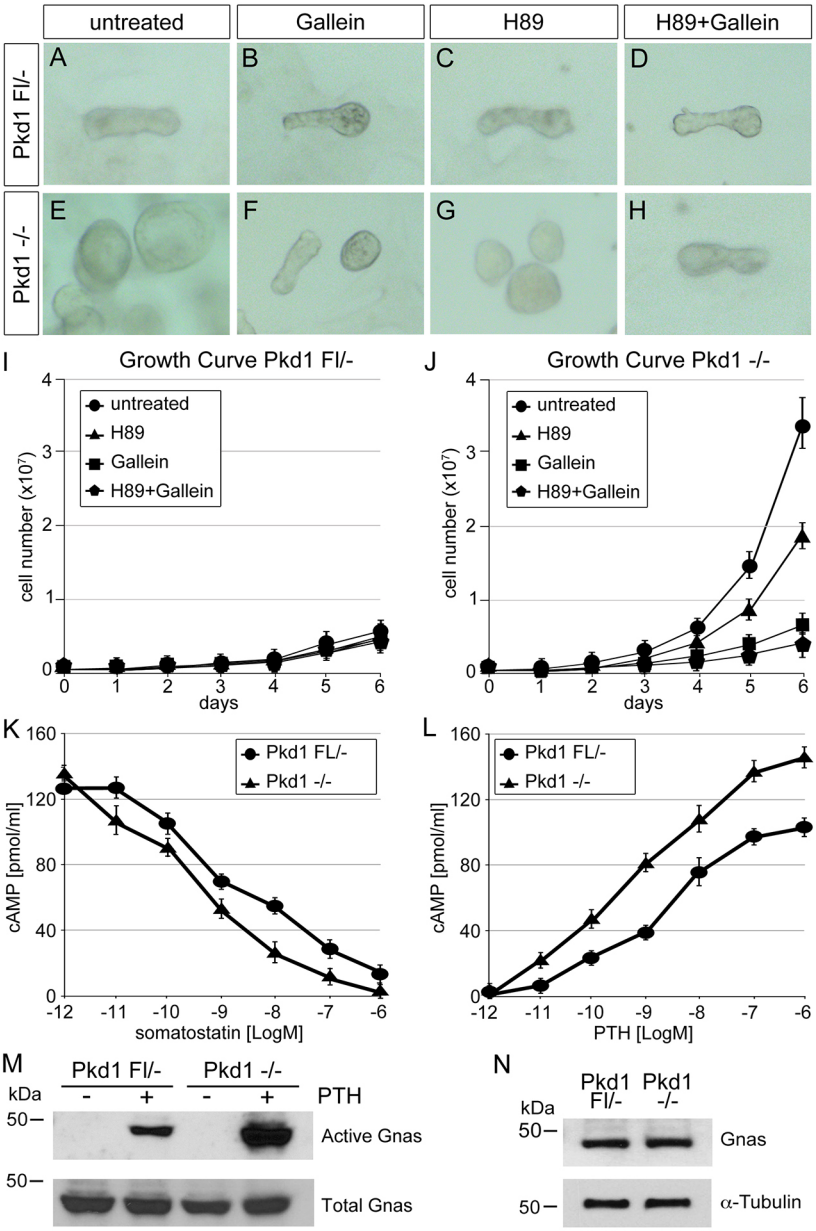

Fig. 6. The *Pkd1* mutant mouse proximal tubular cells upregulation GPCR signaling. (A-J) 3D-Matrigel assay (A-H) and growth curves (I,J) of the isogenic *Pkd1*$^{Fl/-}$ and *Pkd1*$^{-/-}$ cells in the presence or absence of 5 µM H89, 5 µM gallein or a combination of both. (K,L) Dose-response curves for the inhibition of cAMP production by somatostatin (K) or the activation of it by parathyroid hormone (PTH) (L) comparing *Pkd1*$^{Fl/-}$ and *Pkd1*$^{-/-}$ cells. (M) Western blot analysis of immunoprecipitated Gnas using both a total and an activated Gnas antibody demonstrates increased levels of GTP-bound Gnas in response to 10^{-6} M PTH. (N) Western blot analysis examining total Gnas levels between the two cell lines.

combination of both was most potent, blunting proliferation to the baseline levels seen in the Pkd1-expressing isogenic controls.

Next, we directly assessed whether G-protein signaling is upregulated in the absence of Pkd1. To achieve this, we interrogated the activity of Gnas or Gnai using changes in cAMP levels as readout for these two G-protein families. Activation of the Gnai family by the specific agonist somatostatin caused a concentration-dependent decrease in cAMP levels (Fig. 6K). This dose-response curve was shifted in the *Pkd1*$^{-/-}$ cells. Mutant cells were about 10-fold more sensitive to somatostatin when compared with control cells. The same hypersensitivity was observed with parathyroid hormone (PTH), which activates Gnas. A given concentration of PTH had a more pronounced effect on cAMP levels in mutant than in control cells (Fig. 6L). To verify that the latter effect was indeed due to hyperactivation of Gnas, we immunoprecipitated Gnas from cells in the presence or absence of PTH, and analyzed it using an antibody specifically recognizing activated GTP-bound Gnas. Overall levels of Gnas were identical in both cell types (Fig. 6M,N). Yet upon PTH stimulation, higher levels of activated Gnas were detected in *Pkd1*$^{-/-}$ cells than in the isogenic control cells. Together our data support the model that loss of Pkd1 changes the cellular response to GPCR-mediated signaling.

DISCUSSION

Recent structural analyses of PKD1 have suggested that Pkd1 is an aGPCR (Trudel et al., 2016). This is based on the analysis of the GPCR auto-proteolysis site (GPS), which turned out to be part of a larger domain, the GPCR autoproteolysis-inducing (GAIN) domain characteristic of adhesion GPCRs (aGPCRs), the second largest subgroup of GPCRs (Langenhan et al., 2013; Prömel et al., 2013; Trudel et al., 2016). One interesting feature of aGPCRs is that only some of them seem to signal via G-proteins (Gupte et al., 2012), instead they use a range of other signaling modalities (reviewed by Langenhan et al., 2013). This is similar to Pkd1 itself. Early studies have focused on the connection between PKD1 and G proteins, which was then supplanted by the identification and

Development (2018) 145, dev158931. doi:10.1242/dev.158931

characterization of many other signaling moieties (for a review, see Harris and Torres, 2014; Hama and Park, 2016). Yet consensus has not been reached over whether G-protein-mediated signaling by PKD1 is functionally relevant.

Using the pronephric kidney of *Xenopus* as a model system, we now provide new evidence for the interaction between Pkd1 and G proteins. This interpretation is based on five key observations: (1) in contrast to the complete intracellular C-terminal tail, a construct lacking the G-protein binding domain (GBD) is unable to rescue Pkd1 morphants; (2) the C-terminal tail binds a select class of G-protein α subunits (i.e. Gnas, Gnai1, Gnai2, Gna12 and Gna14) at affinities in a range similar to those observed for other GPCRs; (3) loss-of-function studies for these G-protein α subunits (but none of the others) display a PKD phenotype in *Xenopus* embryos that is highly similar to the one observed for Pkd1; (4) the phenotype of Pkd1 morphants can be reversed by inhibiting downstream G-protein β/γ signaling, demonstrating that the interaction between Pkd1 and G proteins is functionally relevant; (5) the mechanism is evolutionarily conserved as it is observed not only in *Xenopus*, but also in murine renal epithelial cells that lack Pkd1. These data demonstrate that a crucial functional domain of PKD1 resides within its GBD.

One conundrum of the data presented here is that the amount of cellular polycystin 1 is believed to be rather low in comparison with the G-proteins. Thus, the observed imbalance in G-protein signaling probably only occurs when polycystin 1 is in close proximity to other GPCRs. Two such spatially confined subcellular compartments are lipid rafts and cilia. In particular, the latter has been implicated in PKD (Avasthi et al., 2017; Ma et al., 2017; Pala et al., 2017). Both GPCRs and polycystin 1 are present in cilia (Yoder et al., 2002; Schou et al., 2015; Hilgendorf et al., 2016). Moreover, the cilia localization of polycystin 1 is crucial for the development of a fully established cystic phenotype (Ma et al., 2013). Interestingly, Ma et al. (2017) proposes a cilia-dependent cyst activation (CDCA) signaling pathway, but the nature of it is still unknown. In future, it will be interesting to see whether part of the CDCA is the crosstalk between polycystin 1 and GPCRs in cilia.

One major issue not resolved in this study is whether and how PKD1 itself activates trimeric G-protein signaling activity. aGPCRs can be activated by multiple means that mostly involve the cleavage of the protein at the GPS site and activities residing either in the N- or the C-terminal fragment (Langenhan et al., 2013; Prömel et al., 2013). In the kidney, fluid flow has long been thought to be the primary trigger for PKD1 activation, but other mechanisms, such as polycystin 1 acting as a WNT receptor, are emerging (Kim et al., 2016). Our experiments with pharmacological activators (Fig. 4) did not identify an active the GPCR signaling role for Pkd1. But as this is a negative result, we cannot exclude the possibility that a secondary messenger exists that is activated downstream of polycystin 1. Importantly, such a function would need to be a phenotype that we have not yet described for the Pkd1 morphants or is so subtle that it is overshadowed by the G-protein squelching aspect of the phenotype. Regardless, the most definitive answer will likely come from genetic studies in mouse. Unfortunately, mouse mutants of trimeric G proteins have been poorly studied for their function in the kidney. With respect to the G proteins identified in this study, Gnas, Gnai2 and Gnb1 are lethal or severely growth retarded (Yu et al., 1998; Fu et al., 2006; Okae and Iwakura, 2010), Gnai1 has not been analyzed for its kidney function or explored because compound mutants with Gnai2 (Pineda et al., 2004) and Gnai14 mutants are not available.

This study has direct implications for our understanding of autosomal dominant polycystic kidney disease (ADPKD). Mutations in polycystin 1 account for 70% of all individuals diagnosed with ADPKD. Cyst formation and expansion in ADPKD has long been correlated with an increase in GPCR signaling. In fact, the most promising therapeutic approach so far is the use of the vasopressin receptor (V2R) antagonist tolvaptan (Torres et al., 2012). Although it has been proposed that the increase in vasopressin signaling is a consequence of a defect in calcium homeostasis, we now propose a more direct model. Loss of polycystin 1 increases the pool of available G proteins and allows other GPCRs (such as V2R) to recruit them. As a consequence, these GPCRs can now be overactivated – obviously in the presence of appropriate ligands. It is also noteworthy that polycystin 1 does not bind all G-protein α subunits. Instead, it binds only a selected group (one or two from each family) and thus loss of polycystin 1 will not hyper-activate all GPCR signaling.

Our model also explains the pleiotropic nature of the PKD phenotype. Different organs have different assortments of GPCRs and although, for example, vasopressin/V2R signaling is abundant in the kidney, it is not present in the liver. This obviously also has implications for the development of future therapeutic agents. Reducing certain GPCR signaling pathways may be more easily achievable than interfering with ubiquitous second messengers such as Ca^{2+}. The beneficial effect of vasopressin antagonism on kidney cysts (Torres et al., 2012) may just be the first successfully targeted GPCR to alleviate the multiple organ manifestations of ADPKD.

Another conclusion from our study is that G-protein β/γ signaling in PKD is more crucial than generally thought. In G-protein signaling, the contributions of G-β/γ-dependent signaling are often overlooked, even though they are involved in multiple aspects of GPCR-mediated signaling and regulation (Clapham and Neer, 1997; Smrcka, 2008; Dupre et al., 2009). Early studies have shown that PKD1 bound to Gnai/Gnao regulates Ca^{2+} and K^{+} channels via a G-protein β/γ-dependent mechanism (Delmas et al., 2002, 2004). More recently, another modulator of G-protein β/γ signaling, the activator of G-protein signaling 3 (AGS3) has been implicated in PKD (Kim et al., 1999; Nadella et al., 2010). AGS3 acts as a guanine dinucleotide dissociation inhibitor by binding to inactive Gnai and Gnao, and thereby liberates the G-protein β/γ subunits. These, in turn, regulate PKD2 channel activity and cell proliferation. Interestingly, as in the present study, the effects of AGS3 can be, at least in acute kidney injury, inhibited by addition of the G-protein β/γ signaling inhibitor gallein (Regner et al., 2011). In fact, there has been an emerging interest in targeting G-protein β/γ signaling for clinical intervention in multiple diseases such as heart failure or acute kidney injury (Lin and Smrcka, 2011; White et al., 2014; Bernardo and Blaxall, 2016). Especially as gallein and its derivatives do not cause obvious side effects in mice (Lin and Smrcka, 2011). Thus, inhibiting β/γ signaling in conjunction with other, for example, G-protein α inhibitors may be a future possibility for PKD therapy.

MATERIALS AND METHODS

Embryo manipulations

Xenopus experiments were approved by the Institutional Animal Care and Use Committee (IACUC) and adhered to the National Institutes of Health Guide for the Care and Use of Laboratory Animals. All experiments in this study were performed using *Xenopus laevis* embryos obtained by *in vitro* fertilization, maintained in 0.1× modified Barth medium (Sive et al., 2000) and staged according to Nieuwkoop and Faber (1994). Antisense morpholino oligomers (MOs) were obtained from GeneTools. The sequences of the MOs are summarized in Table S1. MOs were diluted to a concentration of 1 mM. To target both of the homologs of *Gna14*, the two

Development (2018) 145, dev158931. doi:10.1242/dev.158931

MOs were mixed at a 1:1 ratio. The targeting efficacy for newly designed MOs was verified using *in vitro* transcription/translation using the Retic Lysate IVT Kit (Ambion) in the presence of Transcend tRNA.

For all the injections, a total of 8 nl of morpholino oligomer solution was injected radially at the two- to four-cell stage into *Xenopus laevis* embryos. At the onset of our study, only *Xenopus tropicalis* polycystin 1 had been identified and cloned. Therefore, the *pCS2-Pkd1-CTT* construct was generated by PCR using a *Xenopus tropicalis* polycystin 1 EST (Image# 7650819); the *pCS2-Pkd1-CTTΔGBD* was generated using the QuikChange II Site-Directed Mutagenesis Kit (Agilent) deleting the core G-protein-binding domain (GBD), i.e. the five amino acids RHKVR. For synthetic mRNA, all plasmids were linearized with *Not*I and transcribed with SP6 RNA polymerase using the mMessage mMachine (Ambion). For the rescue experiments, the *Pkd1-sMO* was injected radially at the two- to four-cell stage followed by two injections of 2 ng synthetic mRNA into one vegetal blastomere at the eight-cell stage.

For the drug experiments, *Xenopus* embryos were cultured until stage 20, when polycystin 1 mRNA expression can first be detected. At this time point, injected and uninjected controls were treated with the indicated amounts of the chemical compounds by simply adding the compounds to the medium; drugs were exchanged every 24 h and embryos were fixed when the untreated controls reached stage 39 or 42. Brefeldin A (BFA), forskolin and H89 were obtained from Sigma, 6-Bnz-cAMP-AM (cAMP-PKA) and the 8-pCPT-2′-O-Me-cAMP-AM (cAMP-Epac) were obtained from Biolog, and gallein and m-3M3FBS were obtained from Calbiochem. For all the drug experiments, we carefully titrated the compounds using a wide concentration range, as the IC_{50} concentration is often not equivalent to the EC_{50}. One important note of caution is that the quality of gallein is very batch/supplier-dependent and needs to be carefully titrated.

Whole-mount *in situ* hybridization and histology

In situ hybridization and its analysis by paraplast sectioning and several antisense probes have been described previously (Belo et al., 1997; Zhou and Vize, 2004; Tran et al., 2007). The information for the novel antisense probes is summarized in Table S1. For histological staining, *Xenopus* embryos were fixed in Bouin's fixative, dehydrated, embedded in paraplast, sectioned at 7 µm, dewaxed and stained with Hematoxylin and Eosin.

Cell culture studies

All cells are tested every 6 months for mycoplasma contamination. The nuclear localization studies were performed in HEK293T cells (ATCC) transiently transfected with a Myc-tagged version of Pkd1-CTT or Pkd1-CTTΔGBD using jetPRIME (Polyplus Transfections). 48 h after transfection, cells were processed for immunofluorescence using the mouse anti-Myc antibody (clone 9E10, DSHB, 1:50) and an Alexa Fluor-647-coupled secondary antibody (#A31571, Life Technologies, 1:2000). Images were analyzed by confocal microscopy and analyzed by LAS X (Leica Microsystems).

The two isogenic proximal tubular cell lines $Pkd1^{Fl/-}$ and $Pkd1^{-/-}$ were a kind gift from Dr S. Somlo (Shibazaki et al., 2008). Cells were propagated at 33°C, but all experiments were performed at the non-permissive temperature of 37°C. The 3D matrigel cultures were set up as previously described (Merrick et al., 2012). Drugs were added the next day, replaced every 24 h and cells were imaged after 7 days in culture. For the proliferation assay, 200,000 cells were seeded into a 10 cm plate, grown for 24 h, counted using the Beckman Z2 Coulter and 200,000 cells were then re-seeded; the growth curve was calculated based on the daily dilution factors.

To measure cAMP levels upon somatostatin treatment, cells were starved overnight in DMEM/F12, treated with 10 µM forskolin for 10 min and then stimulated with different concentrations of somatostatin (Calbiochem) for 30 min. cAMP levels were determined using the Direct cAMP ELISA kit (ENZO). For the parathyroid hormone (PTH) assay, cells were starved overnight in DMEM/F12, treated with different concentrations of PTH in the presence of 1 mM IBMX (to prevent cAMP degradation) for 15 min and analyzed as described above.

To determine the levels of activated GTP-bound Gnas, cells were starved overnight in DMEM/F12 and treated with 10^{-6} M PTH. Cell lysates were used for immunoprecipitation using the activated Gnas antibody (#26906, NewEast Biosciences) and analyzed by western blot using a Gnas-specific antibody (#sc-823, Santa Cruz Biotechnologies, 1:500). The same antibody was used for determining total Gnas levels. Equal loading was confirmed using an α-tubulin antibody (#T9026, Sigma, 1:2000).

Determination of the orientation of cell division

As the amount of mitotic cells in the developing pronephric kidney (i.e. phospho Histone H3-positive) at a given time is rather low, we used pulse labeling with EdU to follow the fate of cells after cell division. *Xenopus* embryos were injected at stage 40 with 8 nl EdU stock solution into the belly and cultured until stage 42. Embryos were fixed in 4% PFA and processed for paraplast sectioning. To determine whether cells divided along the length of the pronephros or circumferentially, embryos were sectioned either transverse or sagittally. They were then de-waxed, rehydrated and re-fixed in 4% PFA for 15 min. Staining was performed as outlined in the instructions of the Click-iT EdU imaging kit (Thermo Fisher Scientific) using 500 µl per slide for 30 min. Wash the slides briefly with 3% BSA. To distinguish cells of the pronephric kidney from the surrounding interstitium, sections were then subjected to immunofluorescence staining using anti α-Na/K ATPase (clone #A5, DSHB, 1:50) and anti mouse Alexa Fluor-488 (#A11001, Life Technologies, 1:2000). Slides were mounted in Prolong Gold with DAPI (Thermo Fisher Scientific) and analyzed by fluorescence microscopy and analyzed by LAS X (Leica Microsystems). For all sections containing cells of the pronephros, the frequency of duplets of EdU-labeled daughter cells among the total number of Na/K ATPase and DAPI-positive cells were determined. Cells that were not present as EdU-labeled duplets were not considered to have divided in the plane of the section and were not included in the counts.

Surface plasmon resonance analysis

Binding affinities between the C-terminal tail of Pkd1 and different G-protein α subunits were determined using the BIAcore 3000. The different G-protein α subunits were generated using *in vitro* transcription/translation as outlined above and bound to a streptavidin chip. Protein quality was confirmed by western blot and equal binding to the chip was determined by comparing the baselines (Fig. S4). The Pkd1-CTT and Pkd1-CTTΔGBD proteins were produced as GST-fusion proteins, purified using glutathione beads and cleaved off from the GST-tag using ProTEV Plus (Promega). Protein integrity and amount were determined using the BSA standards of the BCA Protein Assay Kit (Thermo) and Coomassie Blue staining. To determine association and dissociation constants, different concentrations (0.1 ng/ml to 100 ng/ml) were used. In order to confirm the binding affinities, the experiment was also performed in reverse; GST-Pkd1-CTT and GST-Pkd1-CTTΔGBD were bound to a CM5 chip coupled with a GST antibody (#06-332, Millipore) and different concentrations of GST-purified Gnas (0.1 ng/ml to 100 ng/ml) were used.

Methodology and statistics

All experiments were performed a minimum of three times. All data from the *Xenopus* experiments were repeated using clutches of eggs from different females and independent fertilizations. The group size in each individual experiment was ≥25 embryos/condition and the sex of the embryos was undetermined. For the drug exposure experiments, injected and uninjected embryos were randomly divided into the experimental groups. As in all our *Xenopus* experiments, embryos that did not gastrulate properly or showed severe developmental abnormalities were discarded. All other embryos were used for the data analysis. The *Xenopus* data are presented as cumulative numbers with the number of embryos analyzed presented above the individual bars. Figures showing *in situ* hybridization (whole mount and sections thereof), as well as fluorescence and light-field microscopy are representative images.

Acknowledgements

We thank Drs M. Blum, J. Larraín, E. Pera and S. Piccolo, as well as all members of the laboratory for critically reviewing the manuscript and helpful discussions.

Competing interests

The authors declare no competing or financial interests.

Author contributions
Conceptualization: O.W.; Formal analysis: B.Z., U.T., O.W.; Investigation: B.Z., U.T., O.W.; Writing - original draft: B.Z., U.T., O.W.; Writing - review & editing: B.Z., U.T., O.W.; Visualization: B.Z., U.T., O.W.; Supervision: O.W.; Project administration: O.W.; Funding acquisition: O.W.

Funding
The Molecular Biotechnology Core at the Lerner Research Institute/Cleveland Clinic is supported by a grant from National Institutes of Health/National Center for Research Resources to Dr Satya P. Yadav (1S10RR016789-01A1). This work was supported by a grant from National Institutes of Health/National Institute of Diabetes and Digestive and Kidney Diseases (5R01DK080745) and an Lerner Research Institute Chair's Innovative Research Fund to O.W. Deposited in PMC for release after 12 months.

Supplementary information
Supplementary information available online at
http://dev.biologists.org/lookup/doi/10.1242/dev.158931.supplemental

References

Avasthi, P., Maser, R. L. and Tran, P. V. (2017). Primary cilia in cystic kidney disease. *Results Probl. Cell Differ.* **60**, 281-321.
Belo, J. A., Bouwmeester, T., Leyns, L., Kertesz, N., Gallo, M., Follettie, M. and De Robertis, E. M. (1997). *Cerberus-like* is a secreted factor with neutralizing activity expressed in the anterior primitive endoderm of the mouse gastrula. *Mech. Dev.* 68, 45-57.
Bernardo, B. C. and Blaxall, B. C. (2016). From bench to bedside: new approaches to therapeutic discovery for heart failure. *Heart Lung Circ.* **25**, 425-434.
Bertram, J. F., Cullen-McEwen, L. A., Egan, G. F., Gretz, N., Baldelomar, E., Beeman, S. C. and Bennett, K. M. (2013). Why and how we determine nephron number. *Pediatr. Nephrol.* **29**, 575-580.
Bubenshchikova, E., Ichimura, K., Fukuyo, Y., Powell, R., Hsu, C., Morrical, S. O., Sedor, J. R., Sakai, T. and Obara, T. (2012). Wtip and Vangl2 are required for mitotic spindle orientation and cloaca morphogenesis. *Biol. Open* **1**, 588-596.
Cai, Y., Fedeles, S. V., Dong, K., Anyatonwu, G., Onoe, T., Mitobe, M., Gao, J. D., Okuhara, D., Tian, X., Gallagher, A.-R. et al. (2014). Altered trafficking and stability of polycystins underlie polycystic kidney disease. *J. Clin. Invest.* **124**, 5129-5144.
Calvet, J. P. (2015). The role of calcium and cyclic AMP in PKD. In *Polycystic Kidney Disease* (ed. X. Li), pp. 169-196. Brisbane, Australia: Codon Publications.
Chauvet, V., Tian, X., Husson, H., Grimm, D. H., Wang, T., Hiesberger, T., Igarashi, P., Bennett, A. M., Ibraghimov-Beskrovnaya, O., Somlo, S. et al. (2004). Mechanical stimuli induce cleavage and nuclear translocation of the polycystin-1 C terminus. *J. Clin. Invest.* **114**, 1433-1443.
Chebib, F. T. and Torres, V. E. (2016). Autosomal dominant polycystic kidney disease: core curriculum 2016. *Am. J. Kidney Dis.* **67**, 792-810.
Clapham, D. E. and Neer, E. J. (1997). G protein beta gamma subunits. *Annu. Rev. Pharmacol. Toxicol.* **37**, 167-203.
Delmas, P., Nomura, H., Li, X., Lakkis, M., Luo, Y., Segal, Y., Fernandez-Fernandez, J. M., Harris, P., Frischauf, A. M., Brown, D. A. et al. (2002). Constitutive activation of G-proteins by polycystin-1 is antagonized by polycystin-2. *J. Biol. Chem.* **277**, 11276-11283.
Delmas, P., Nauli, S. M., Li, X., Coste, B., Osorio, N., Crest, M., Brown, D. A. and Zhou, J. (2004). Gating of the polycystin ion channel signaling complex in neurons and kidney cells. *FASEB J.* **18**, 740-742.
Desgrange, A. and Cereghini, S. (2015). Nephron patterning: lessons from Xenopus, Zebrafish, and mouse studies. *Cells* **4**, 483-499.
Dorsam, R. T. and Gutkind, J. S. (2007). G-protein-coupled receptors and cancer. *Nat. Rev. Cancer* **7**, 79-94.
Dupre, D. J., Robitaille, M., Rebois, R. V. and Hebert, T. E. (2009). The role of Gbetagamma subunits in the organization, assembly, and function of GPCR signaling complexes. *Annu. Rev. Pharmacol. Toxicol.* **49**, 31-56.
Fedeles, S. and Gallagher, A. R. (2013). Cell polarity and cystic kidney disease. *Pediatr. Nephrol.* **28**, 1161-1172.
Fischer, E., Legue, E., Doyen, A., Nato, F., Nicolas, J. F., Torres, V., Yaniv, M. and Pontoglio, M. (2006). Defective planar cell polarity in polycystic kidney disease. *Nat. Genet.* **38**, 21-23.
Fu, Y., Huang, X., Zhong, H., Mortensen, R. M., D'Alecy, L. G. and Neubig, R. R. (2006). Endogenous RGS proteins and Galpha subtypes differentially control muscarinic and adenosine-mediated chronotropic effects. *Circ. Res.* **98**, 659-666.
Grantham, J. J., Mulamalla, S. and Swenson-Fields, K. I. (2011). Why kidneys fail in autosomal dominant polycystic kidney disease. *Nat. Rev. Nephrol.* **7**, 556-566.
Gupte, J., Swaminath, G., Danao, J., Tian, H., Li, Y. and Wu, X. (2012). Signaling property study of adhesion G-protein-coupled receptors. *FEBS Lett.* **586**, 1214-1219.
Hama, T. and Park, F. (2016). Heterotrimeric G protein signaling in polycystic kidney disease. *Physiol. Genomics* **48**, 429-445.
Happé, H. and Peters, D. J. M. (2014). Translational research in ADPKD: lessons from animal models. *Nat. Rev. Nephrol.* **10**, 587-601.
Harris, P. C. and Torres, V. E. (2009). Polycystic kidney disease. *Annu. Rev. Med.* **60**, 321-337.
Harris, P. C. and Torres, V. E. (2014). Genetic mechanisms and signaling pathways in autosomal dominant polycystic kidney disease. *J. Clin. Invest.* **124**, 2315-2324.
Hilgendorf, K. I., Johnson, C. T. and Jackson, P. K. (2016). The primary cilium as a cellular receiver: organizing ciliary GPCR signaling. *Curr. Opin. Cell Biol.* **39**, 84-92.
Hughes, J., Ward, C. J., Peral, B., Aspinwall, R., Clark, K., San Millán, J. L., Gamble, V. and Harris, P. C. (1995). The polycystic kidney disease 1 (PKD1) gene encodes a novel protein with multiple cell recognition domains. *Nat. Genet.* **10**, 151-160.
Karner, C. M., Chirumamilla, R., Aoki, S., Igarashi, P., Wallingford, J. B. and Carroll, T. J. (2009). Wnt9b signaling regulates planar cell polarity and kidney tubule morphogenesis. *Nat. Genet.* **41**, 793-799.
Kim, E., Arnould, T., Sellin, L., Benzing, T., Comella, N., Kocher, O., Tsiokas, L., Sukhatme, V. P. and Walz, G. (1999). Interaction between RGS7 and polycystin. *Proc. Natl. Acad. Sci. USA* **96**, 6371-6376.
Kim, S., Nie, H., Nesin, V., Tran, U., Outeda, P., Bai, C.-X., Keeling, J., Maskey, D., Watnick, T., Wessely, O. et al. (2016). The polycystin complex mediates Wnt/Ca(2+) signalling. *Nat. Cell Biol.* **18**, 752-764.
Komolov, K. E., Senin, I. I., Philippov, P. P. and Koch, K.-W. (2006). Surface plasmon resonance study of g protein/receptor coupling in a lipid bilayer-free system. *Anal. Chem.* **78**, 1228-1234.
Kurbegovic, A., Kim, H., Xu, H., Yu, S., Cruanes, J., Maser, R. L., Boletta, A., Trudel, M. and Qian, F. (2014). Novel functional complexity of polycystin-1 by GPS cleavage in vivo: role in polycystic kidney disease. *Mol. Cell. Biol.* **34**, 3341-3353.
Langenhan, T., Aust, G. and Hamann, J. (2013). Sticky signaling–adhesion class G protein-coupled receptors take the stage. *Sci. Signal.* **6**, re3.
Lienkamp, S. S., Liu, K., Karner, C. M., Carroll, T. J., Ronneberger, O., Wallingford, J. B. and Walz, G. (2012). Vertebrate kidney tubules elongate using a planar cell polarity-dependent, rosette-based mechanism of convergent extension. *Nat. Genet.* **44**, 1382-1387.
Lin, Y. and Smrcka, A. V. (2011). Understanding molecular recognition by G protein betagamma subunits on the path to pharmacological targeting. *Mol. Pharmacol.* **80**, 551-557.
Low, S. H., Vasanth, S., Larson, C. H., Mukherjee, S., Sharma, N., Kinter, M. T., Kane, M. E., Obara, T. and Weimbs, T. (2006). Polycystin-1, STAT6, and P100 function in a pathway that transduces ciliary mechanosensation and is activated in polycystic kidney disease. *Dev. Cell* **10**, 57-69.
Ma, M., Gallagher, A. R. and Somlo, S. (2017). Ciliary mechanisms of cyst formation in polycystic kidney disease. *Cold Spring Harb. Perspect. Biol.* **9**, a0282209.
Ma, M., Tian, X., Igarashi, P., Pazour, G. J. and Somlo, S. (2013). Loss of cilia suppresses cyst growth in genetic models of autosomal dominant polycystic kidney disease. *Nat. Genet.* **45**, 1004-1012.
McMahon, A. P. (2016). Development of the mammalian kidney. *Curr. Top. Dev. Biol.* **117**, 31-64.
Merrick, D., Chapin, H., Baggs, J. E., Yu, Z., Somlo, S., Sun, Z., Hogenesch, J. B. and Caplan, M. J. (2012). The gamma-secretase cleavage product of polycystin-1 regulates TCF and CHOP-mediated transcriptional activation through a p300-dependent mechanism. *Dev. Cell* **22**, 197-210.
Mochizuki, T., Wu, G., Hayashi, T., Xenophontos, S. L., Veldhuisen, B., Saris, J. J., Reynolds, D. M., Cai, Y., Gabow, P. A., Pierides, A. et al. (1996). PKD2, a gene for polycystic kidney disease that encodes an integral membrane protein. *Science* **272**, 1339-1342.
Nadella, R., Blumer, J. B., Jia, G., Kwon, M., Akbulut, T., Qian, F., Sedlic, F., Wakatsuki, T., Sweeney, W. E., Jr, Wilson, P. D. et al. (2010). Activator of G protein signaling 3 promotes epithelial cell proliferation in PKD. *J. Am. Soc. Nephrol.* **21**, 1275-1280.
Neves, S. R., Ram, P. T. and Iyengar, R. (2002). G protein pathways. *Science* **296**, 1636-1639.
Nieuwkoop, P. D. and Faber, J. (1994). *Normal Table of Xenopus Laevis*. New York: Garland Publishing, Inc.
Nishio, S., Tian, X., Gallagher, A. R., Yu, Z., Patel, V., Igarashi, P. and Somlo, S. (2010). Loss of oriented cell division does not initiate cyst formation. *J. Am. Soc. Nephrol.* **21**, 295-302.
Okae, H. and Iwakura, Y. (2010). Neural tube defects and impaired neural progenitor cell proliferation in Gbeta1-deficient mice. *Dev. Dyn.* **239**, 1089-1101.
Pala, R., Alomari, N. and Nauli, S. M. (2017). Primary cilium-dependent signaling mechanisms. *Int. J. Mol. Sci.* **18**, 2272.
Parnell, S. C., Magenheimer, B. S., Maser, R. L., Rankin, C. A., Smine, A., Okamoto, T. and Calvet, J. P. (1998). The polycystic kidney disease-1 protein, polycystin-1, binds and activates heterotrimeric G-proteins in vitro. *Biochem. Biophys. Res. Commun.* **251**, 625-631.
Parnell, S. C., Magenheimer, B. S., Maser, R. L., Zien, C. A., Frischauf, A.-M. and Calvet, J. P. (2002). Polycystin-1 activation of c-Jun N-terminal kinase and AP-1 is mediated by heterotrimeric G proteins. *J. Biol. Chem.* **277**, 19566-19572.

Pineda, V. V., Athos, J. I., Wang, H., Celver, J., Ippolito, D., Boulay, G., Birnbaumer, L. and Storm, D. R. (2004). Removal of G(ialpha1) constraints on adenylyl cyclase in the hippocampus enhances LTP and impairs memory formation. *Neuron* **41**, 153-163.

Prömel, S., Langenhan, T. and Arac, D. (2013). Matching structure with function: the GAIN domain of adhesion-GPCR and PKD1-like proteins. *Trends Pharmacol. Sci.* **34**, 470-478.

Qian, F. (2015). The role of G-protein coupled receptor proteolytic site (GPS) cleavage in polycystin-1 biogenesis, trafficking and function. In *Polycystic Kidney Disease* (ed. X. Li), pp. 259-281. Brisbane, Australia: Codon Publications.

Regner, K. R., Nozu, K., Lanier, S. M., Blumer, J. B., Avner, E. D., Sweeney, W. E., Jr and Park, F. (2011). Loss of activator of G-protein signaling 3 impairs renal tubular regeneration following acute kidney injury in rodents. *FASEB J.* **25**, 1844-1855.

Romaker, D., Kumar, V., Cerqueira, D. M., Cox, R. M. and Wessely, O. (2014). MicroRNAs are critical regulators of tuberous sclerosis complex and mTORC1 activity in the size control of the Xenopus kidney. *Proc. Natl. Acad. Sci. USA* **111**, 6335-6340.

Saxén, L. (1987). *Organogenesis of the Kidney*. Cambridge, UK: Cambridge University Press.

Schou, K. B., Pedersen, L. B. and Christensen, S. T. (2015). Ins and outs of GPCR signaling in primary cilia. *EMBO Rep.* **16**, 1099-1113.

Shibazaki, S., Yu, Z., Nishio, S., Tian, X., Thomson, R. B., Mitobe, M., Louvi, A., Velazquez, H., Ishibe, S., Cantley, L. G. et al. (2008). Cyst formation and activation of the extracellular regulated kinase pathway after kidney specific inactivation of Pkd1. *Hum. Mol. Genet.* **17**, 1505-1516.

Sive, H. L., Grainger, R. M. and Harland, R. M. (2000). *Early Development of Xenopus Laevis: A Laboratory Manual*. Cold Spring Harbor, New York: Cold Spring Harbor Laboratory Press.

Smith, H. W. (1953). *From Fish to Philosopher*. Boston: Little, Brown.

Smrcka, A. V. (2008). G protein betagamma subunits: central mediators of G protein-coupled receptor signaling. *Cell. Mol. Life Sci.* **65**, 2191-2214.

Su, X., Wu, M., Yao, G., El-Jouni, W., Luo, C., Tabari, A. and Zhou, J. (2015). Regulation of polycystin-1 ciliary trafficking by motifs at its C-terminus and polycystin-2 but not by cleavage at the GPS site. *J. Cell Sci.* **128**, 4063-4073.

The International Polycystic Kidney Disease Consortium. (1995). Polycystic kidney disease: the complete structure of the PKD1 gene and its protein. *Cell* **81**, 289-298.

Torres, V. E. and Harris, P. C. (2007). Polycystic kidney disease: genes, proteins, animal models, disease mechanisms and therapeutic opportunities. *J. Intern. Med.* **261**, 17-31.

Torres, V. E., Harris, P. C. and Pirson, Y. (2007). Autosomal dominant polycystic kidney disease. *Lancet* **369**, 1287-1301.

Torres, V. E., Chapman, A. B., Devuyst, O., Gansevoort, R. T., Grantham, J. J., Higashihara, E., Perrone, R. D., Krasa, H. B., Ouyang, J. and Czerwiec, F. S. (2012). Tolvaptan in patients with autosomal dominant polycystic kidney disease. *N Engl. J. Med.* **367**, 2407-2418.

Tran, U., Pickney, L. M., Özpolat, B. D. and Wessely, O. (2007). Xenopus Bicaudal-C is required for the differentiation of the amphibian pronephros. *Dev. Biol.* **307**, 152-164.

Tran, U., Zakin, L., Schweickert, A., Agrawal, R., Doger, R., Blum, M., De Robertis, E. M. and Wessely, O. (2010). The RNA-binding protein bicaudal C regulates polycystin 2 in the kidney by antagonizing miR-17 activity. *Development* **137**, 1107-1116.

Trudel, M., Yao, Q. and Qian, F. (2016). The role of G-protein-coupled receptor proteolysis site cleavage of polycystin-1 in renal physiology and polycystic kidney disease. *Cells* **5**, 3.

Vize, P. D., Woolf, A. and Bard, J. (2003). *The Kidney: From Normal Development to Congenital Diseases*. Amsterdam: Academic Press.

Wessely, O. and Obara, T. (2008). Fish and frogs: models for vertebrate cilia signaling. *Front. Biosci.* **13**, 1866-1880.

Wessely, O. and Tran, U. (2011). Xenopus pronephros development–past, present, and future. *Pediatr. Nephrol.* **26**, 1545-1551.

Wessely, O., Cerqueira, D. M., Tran, U., Kumar, V., Hassey, J. M. and Romaker, D. (2014). The bigger the better: determining nephron size in kidney. *Pediatr. Nephrol.* **29**, 525-530.

White, J. T., Zhang, B., Cerqueira, D. M., Tran, U. and Wessely, O. (2010). Notch signaling, wt1 and foxc2 are key regulators of the podocyte gene regulatory network in Xenopus. *Development* **137**, 1863-1873.

White, S. M., North, L. M., Haines, E., Goldberg, M., Sullivan, L. M., Pressly, J. D., Weber, D. S., Park, F. and Regner, K. R. (2014). G-protein betagamma subunit dimers modulate kidney repair after ischemia-reperfusion injury in rats. *Mol. Pharmacol.* **86**, 369-377.

Xu, Y., Streets, A. J., Hounslow, A. M., Tran, U., Jean-Alphonse, F., Needham, A. J., Vilardaga, J. P., Wessely, O., Williamson, M. P. and Ong, A. C. (2015). The polycystin-1, lipoxygenase, and alpha-toxin domain regulates polycystin-1 trafficking. *J. Am. Soc. Nephrol.* **27**, 1159-1173.

Yoder, B. K., Hou, X. and Guay-Woodford, L. M. (2002). The polycystic kidney disease proteins, polycystin-1, polycystin-2, polaris, and cystin, are co-localized in renal cilia. *J. Am. Soc. Nephrol.* **13**, 2508-2516.

Yu, S., Yu, D., Lee, E., Eckhaus, M., Lee, R., Corria, Z., Accili, D., Westphal, H. and Weinstein, L. S. (1998). Variable and tissue-specific hormone resistance in heterotrimeric Gs protein alpha-subunit (Gsalpha) knockout mice is due to tissue-specific imprinting of the gsalpha gene. *Proc. Natl. Acad. Sci. USA* **95**, 8715-8720.

Yu, W., Kong, T., Beaudry, S., Tran, M., Negoro, H., Yanamadala, V. and Denker, B. M. (2010). Polycystin-1 protein level determines activity of the Galpha12/JNK apoptosis pathway. *J. Biol. Chem.* **285**, 10243-10251.

Yu, W., Ritchie, B. J., Su, X., Zhou, J., Meigs, T. E. and Denker, B. M. (2011). Identification of polycystin-1 and Galpha12 binding regions necessary for regulation of apoptosis. *Cell. Signal.* **23**, 213-221.

Yuasa, T., Takakura, A., Denker, B. M., Venugopal, B. and Zhou, J. (2004). Polycystin-1L2 is a novel G-protein-binding protein. *Genomics* **84**, 126-138.

Zhang, B., Romaker, D., Ferrell, N. and Wessely, O. (2013). Regulation of G-protein signaling via Gnas is required to regulate proximal tubular growth in the Xenopus pronephros. *Dev. Biol.* **376**, 31-42.

Zhou, X. and Vize, P. D. (2004). Proximo-distal specialization of epithelial transport processes within the Xenopus pronephric kidney tubules. *Dev. Biol.* **271**, 322-338.

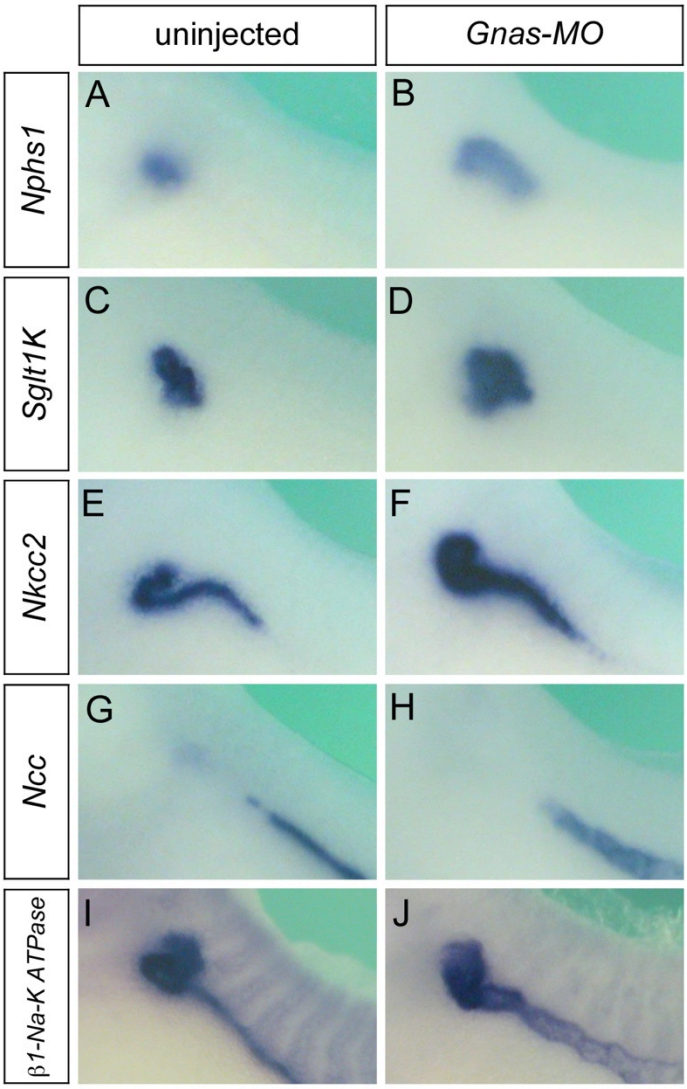

Figure S1: Expression of Proximal-Distal Marker Genes in Gnas Morphants. Whole mount *in situ* hybridization of uninjected control and *Gnas-MO*-injected embryos at stage 39 with *Nphs1* (A,B), *Sglt1K* (C,D), *Nkcc2* (E,F), *Ncc* (G,H) and *β1-Na/K-ATPase* (I,J).

A

```
Human     4081 LSPLLCVGLWALRLWGALRLGAVILRWRYHALRGELYRPAWEPQDYEMVELFLRRLRLWM 4140
X.trop.   4018 ISHLYFASYLVLEVWILLRLFAAVLINSYRQVRLEMFRPAFEPQDYEMVELFLRRLRIWM 4077
               :* *  ..  .*.:*  *** *.:*   *: :* *::***:****************:**

Human     4141 GLSKVKEFRHKVRFEGMEPLPSRSSRGSKVSPDVPPPSAG--SDASHPSTSSSQLDGLSV 4198
X.trop.   4078 GVSKVKEFRHKVRFEGMEPLPSRSSSDSKSIRGLTPSAASDTSSSSSFSTISSQLDSLSA 4137
               *:**********************  .**   .:.*.:*.  *.:*  ** *****.**.

Human     4199 SLGRLGTRCEPEPSRLQAVFEALLTQFDRLNQATEDVYQLEQQLHSLQGRRS-------- 4250
X.trop.   4138 ISARERAEIDANVQRLVPVLDALLSQFDQVNQATEDVYRIECSLEGVQKRASKNRFAKIG 4197
                 .*  :. :.: .** .*::***:***::*********::* .*..:* * *

Human     4251 --------------------SRAPAGSSRGPSPG-------------LRP-ALPSRLARA 4276
X.trop.   4198 KHGRPKTKKSLSNTQLSSGTSRNVAGSQAHLSKPDTHSEVVKDSMQVLRPSTAPQTLVGN 4257
                                    **  ***.   *               *** : *. *.

Human     4277 S-----------RG-------VDLATGPSRTPLRAKNKVHPSST 4302
X.trop.   4258 SGACRVIAVDKARKEEPAMQITNFAQSKKRKSIRAHNRVHPSVS 4301
               *           *        .::* . .*..:**:*:**** :
```

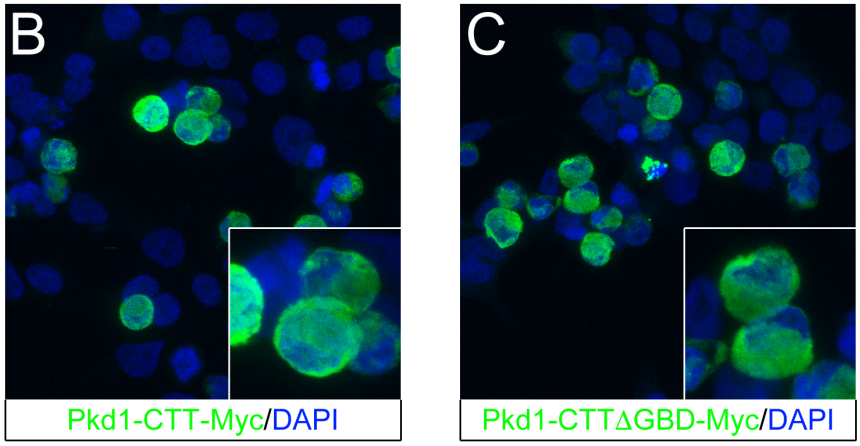

Figure S2: Conservation of the C-terminal Tail of Pkd1. (A) ClustalW alignment of the intracellular domain of Polycystin-1 protein from human (GenBank Accession #NP_000287.3) and *Xenopus tropicalis* (GenBank Accession #XP_002932517.1). Four previously described domains were analyzed. The G-protein binding signature (GBD) is based on the analysis by Parnell et al. (1998). It is indicated in yellow and the domain-identifying amino acids (BB….BBxxB) are bolded. This sequence overlaps with the Nuclear Localization Sequence (NLS) described in Chauvet et al. (2004) and is indicated by a black line above the human sequence. The PEST sequences were identified using *epestfind*. The optimal and predicted domains are indicated in green and turquoise, respectively; the key amino acids identified in Low et al. (2006) are indicated in bold. The coiled-coil domain were identified using *Paircoil2* and are labeled in red. (B,C) Immunofluorescence analysis of HEK293T cells transiently transfected with Pkd1-CTT-Myc (B) or Pkd1-CTTΔGBD-Myc (C). Nuclei were counterstained with DAPI (blue). Insets show close-up of individual cells.

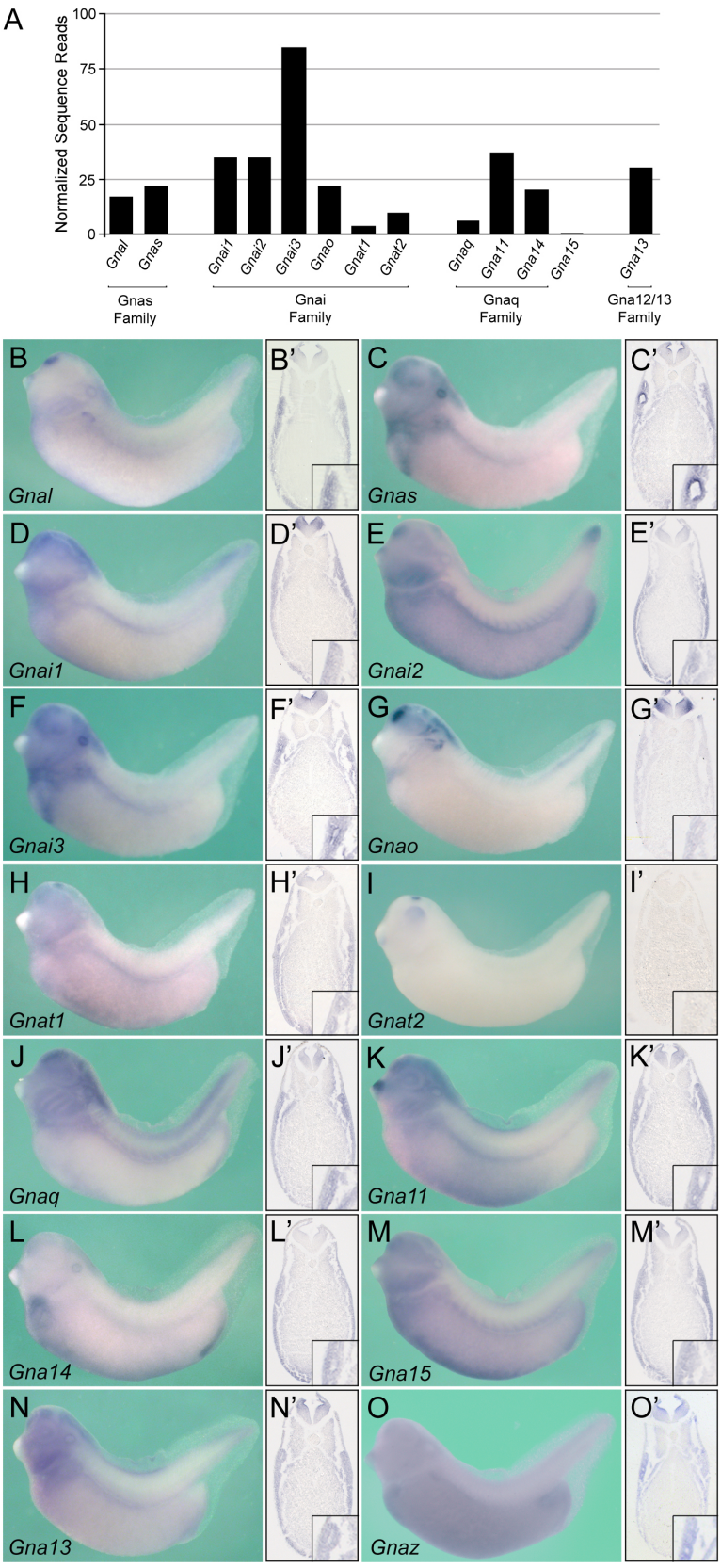

Figure S3: Expression of G-Protein Alpha Subunits in *Xenopus* Embryos. (A) Quantification of the expression levels of G-protein alpha subunits of stage 39 *Xenopus tropicalis* embryos using RNAseq. (B-O') Whole mount *in situ* hybridization of *Xenopus laevis embryos* and paraplast sections thereof demonstrating the expression of G-protein alpha subunits in stage 35 embryos. Insets show close-ups of the pronephric kidney. Note that only *Gnao* (G,G') and *Gnat2* (I,I') are not expressed in the pronephric kidney.

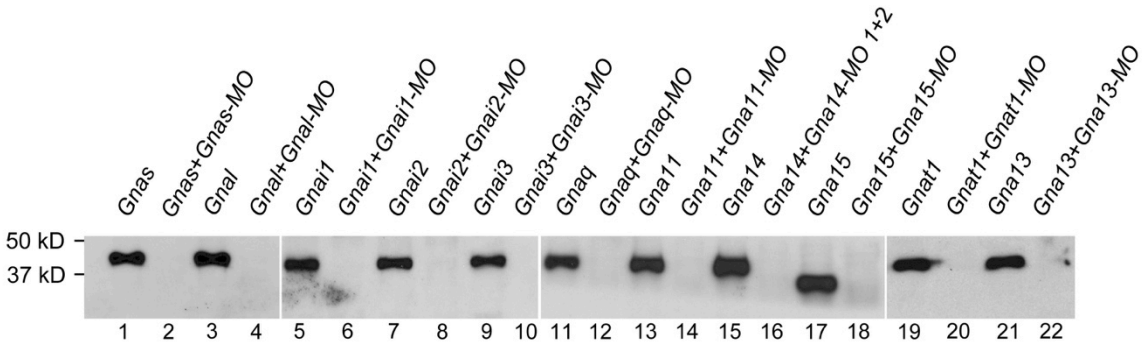

Figure S4: Knockdown of Different G-Protein Alpha Subunits. Analysis of MO knockdown efficacy by *in vitro* transcription/translation.

A

Subunit	Baseline
Gnas	640
Gna14	652
Gnai1	645
Gnai2	655
Gnai3	664
Gna15	701
Gnaq	685
Gnat1	624
Gna11	650
Gnaz	629
Gnal	710
Gna13	648
mGna12	647
Pkd1-CTT	665
Pkd1-CTT(ΔGBD)	672

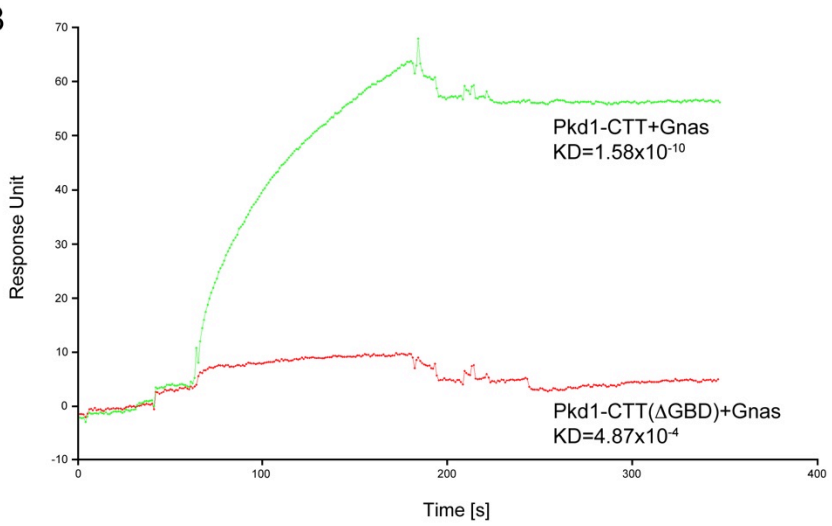

Figure S5: SPR Analysis of the Interaction Between Pkd1 and G-Protein Alpha Subunits. (A) Baseline demonstrating that all the *in vitro* transcribed/translated G-protein alpha subunits were bound to the streptavidin chip in comparable amounts. (B) Representative sensorgram showing the strong interaction of Gnas with a GST-Pkd1-CTT fusion protein, but not with the GST-Pkd1-CTTDGBD. The equilibrium dissociation constants (K_D) for both interactions are shown.

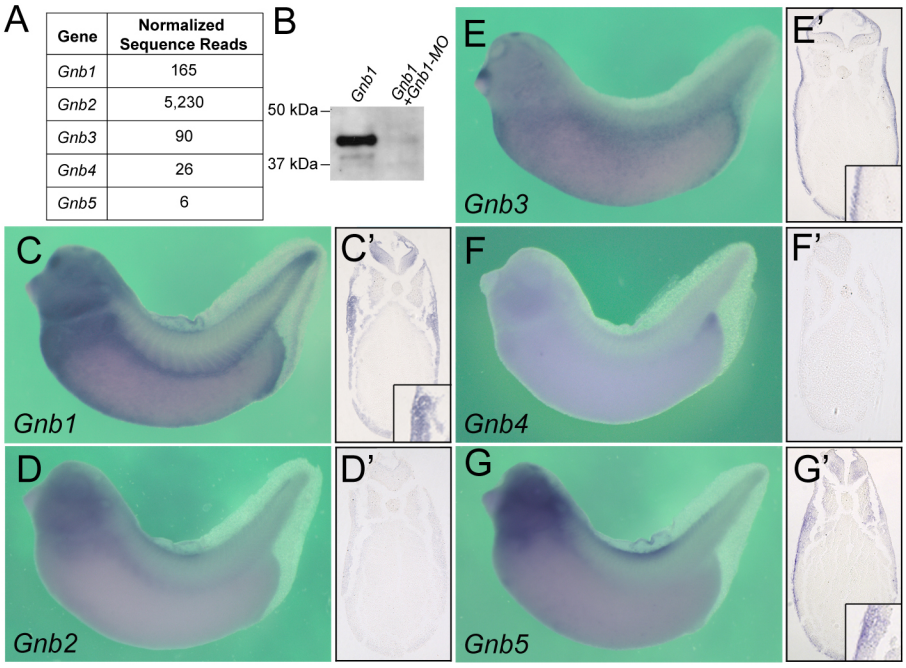

Figure S6: Expression Analysis of G-Protein Beta Subunits. (A) Quantification of the expression levels of G-protein beta subunits of stage 39 *Xenopus tropicalis* embryos using RNAseq. (B) Analysis of *Gnb1-MO* knockdown efficacy by *in vitro* transcription/translation. (C-G') Whole mount *in situ* hybridization of *Xenopus laevis embryos* and paraplast sections thereof demonstrating the expression of G-protein beta subunits in stage 35 embryos. Insets show close-ups of the pronephric kidney. The expression of *Gnb1* in the pronephric kidney was the most pronounced of all the G-Protein beta subunits and was, thus, selected for the knockdown studies.

Table S1: Summary of the Plasmids and MOs.

Antisense Probes for in situ hybridization

Gene	Clone ID	Vector	Antisense	Sense
gnal.S	8317937	pExpress1	T7/EcoRI	Sp6/NotI
gnas.L	6864835	pCMVsport6	T7/Asp718	Sp6/NotI
gnai1.S	8543262	pCS111	T7/PstI	Sp6/NotI
gnai2.S	3404925	pCMVsport6	T7/EcoRI	Sp6/NotI
gnai3.S	8820619	pCS111	T7/PstI	Sp6/NotI
gnao1.L	6947982	pCMVsport6	T7/BamHI	Sp6/NotI
gnat1.L	6950310	pCMVsport6.ccdb	T7/ClaI	Sp6/ApaI
gnat2 (*)	7018744	pCMVsport6	T7/EcoRI	Sp6/NotI
gnaz.S	amplified by PCR	PGEM T-easy	Sp6/NotI	T7/SalI
gnaq.L	8074729	pCS111	T7/EcoRV	Sp6/XhoI
gna11.S	3404901	pCMVsport6	T7/KpnI	Sp6/NotI
gna14.S	5162325	pT7T3D-PacI	T3/XhoI	T7/NotI
gna15.L	8542421	pCS111	T7/ClaI	Sp6/XhoI
gna13.S	6870976	PBlueSk-	T3/KpnI	T7/NotI
gnb1.S	8074931	pExpress1	T7/EcoRV	Sp6/XhoI
gnb2 (*)	7201226	pCMVsport6	T7/SalI	Sp6/NotI
gnb3.S	5571340	pCMVsport6	T7/SalI	Sp6/NotI
gnb4.L	3743760	PBlueSk-	T3/EcoRV	T7/NotI
gnb5.L	6955985	pCMVsport6.ccdb	T7/EcoRV	Sp6/XhoI

(*) genomic sequence information too incomplete to distinguish between S and L.

Antisense Morpholino Oligomers

Gene targeted	MO sequences	Abreviation
gnal.S + gnal.L	5'-CCT AAA CAA CCC ATA TTA ATG GTC C-3'	*Gnal-MO*
gnas.S + gnas.L	5'-AGA CAC CCC ATG GTC CGT GTG GGC T-3'	*Gnas-MO*
gnai1.S + gnai1.L	5'-CTT CGG CGC TCA GAG TAC ATC CCA T-3'	*Gnai1-MO*
gnai2.S + gnai2.L	5'-CAG CGA TAT GTC GCG ACA CAG CCC C-3'	*Gnai2-MO*
gnai3.S + gnai3.L	5'-CCT CGG CAC TCA ATG TGC AGC CCA T-3'	*Gnai3-MO*
gnat1.S + gnat1.L	5'-AGC ACT GGC TCC AGC CCC CAT ATT C-3'	*Gnat1-MO*
gnaq.S + gnaq.L	5'-ACG CCA TGA TGG ACT CCA GAG TCA T-3'	*Gnaq-MO*
gna11.S + gna11.L	5'-TTG AAT CTA GAG TCA TCC CTT CCC C-3'	*Gna11-MO*
gna14.S	5'-GCA GTT GCT GAG TGC GAC CCC TCG C-3'	*Gna14-MO1*
gna14.L	5'-CAA CCC GCC ATG CCC AAG CGC AAT T-3'	*Gna14-MO2*
gna15.S + gna15.L	5'-CAA GGC ATC TTG TAG TAC CAG GTA C-3'	*Gna15-MO*
gna13.S + gna13.L	5'-CAG GAA GTC CGC CAT CTT ACA CAC T-3'	*Gna13-MO*
gnb1.S + gnb1.L	5'-GGC GTA GCT GAT CTA GTT CAC TCA T-3'	*Gnb1-MO*
pkd1.S + pkd1.L	5'-TCC TTA TGG TCC GAG TTA CCT TGG G-3'	*Pkd1-sMO*
pkd2.S + pkd2.L	5'-GGT TTG ATT CTG CTG GGA TTC ATC G-3'	*Pkd2-MO*
rapgef4.S rapgef4.L	5'-CTT GGC GAA ATC CCA TTA CCT CTG T-3'	*Rapgef4-MO*